Syntheses, Structures, and Magnetic Properties of Two 1D, Mixed-Ligand, Metal Coordination Polymers, $[M(C_4O_4)(dpa)(OH_2)]$ ($M = Co^{II}$, Ni^{II}, and Zn^{II}; dpa = 2,2′-dipyridylamine) and $[Cu(C_4O_4)(dpa)(H_2O)]_2\cdot(H_2O)$

Chih-Chieh Wang,*[a] Cheng-Han Yang,[a] Gene-Hsiang Lee,[b] and Hui-Lien Tsai[c]

Keywords: Hydrogen bonds / Hydrothermal synthesis / Magnetic properties / Self-assembly / Squarate

Two metal coordination polymers with general formula $[M(dpa)(C_4O_4)(H_2O)]$ [M = Co (**1**), Ni (**2**), Zn (**3**); dpa = 2,2′-dipyridylamine] and $[Cu(dpa)(C_4O_4)(H_2O)]_2\cdot H_2O$ (**4**) have been synthesized under hydrothermal conditions. The single-crystal X-ray analyses reveal that compounds **1**–**3** are isostructural and possess distorted octahedral metal centers coordinated by two squarates, one dpa, and two water molecules. A 1D two-legged ladder-like framework is formed by interconnection of the water-bridged $[M(dpa)(\mu_2\text{-}OH_2)]_2^{4+}$ dimeric fragments and $\mu_{1,2}$-squarate ligands. Intra- and intermolecular hydrogen bonds between squarate, water, and dpa ligands, as well as the π-π stacking interaction of the pyridyl ring in the dpa ligands, provide extra forces to stabilize the extended network. Conversely, the molecular structure of compound **4** contains two distorted square-pyramidal Cu^{II} centers coordinated by two squarates, one dpa ligand, and one water molecule. The squarates adopt a $\mu_{1,2}$-binding mode to link the Cu centers and form a 1D helical chain. For compound **2**, the magnetic exchange couplings between metal centers are analyzed with a binuclear magnetic model. The resulting negative magnetic exchange coupling constant indicates an antiferromagnetic interaction within the dimers. The magnetic behavior of compound **4** is typical of paramagnetic Cu^{II} ions.

Introduction

Owing to its attractive topologies and intriguing structural features,[1–4] the crystal engineering of mixed-ligand metal coordination solids with functional building blocks has received much attention. Among various methodologies to construct novel 1-, 2-, and 3D frameworks, the hydrothermal method has been ubiquitously applied to the synthesis of metal–organic coordination polymers[5–9] and hydrogen-bonded systems.[10] Of significant important is the ability of the organic molecules to influence profoundly the structures of synthesized products, and to dictate their formation with particular structural and potential applications, such as magnetism, host-guest chemistry, shape specificity, and catalysis. The squarate dianion, $C_4O_4^{2-}$, has been widely used as a polyfunctional ligand, for example to induce hydrogen bonding or π-π interactions, for the construction of extended frameworks and has also been used as a bridging ligand to bind metal ions in various bonding modes to create many novel networks.[11–26] The most typical coordination modes of the squarate dianion are $\mu_{1,2}$- (*cis*) and $\mu_{1,3}$- (*trans*). Many squarate-bridged metal complexes with $\mu_{1,2}$-, $\mu_{1,3}$-, or $\mu_{1,2,3,4}$-binding modes combined with different nitrogen-based flexible ligands have been structurally characterized,[19–25] and their magnetic investigation shows that $\mu_{1,3}$-coordination gives a negligibly small coupling, while $\mu_{1,2}$-coordination induces a small antiferromagnetic coupling.[19,26] In this contribution, we describe the synthesis and structural characterization of two 1D coordination polymers, $[M(dpa)(C_4O_4)(H_2O)]$ [M = Co (**1**), Ni (**2**), Zn (**3**)] and $[Cu(dpa)(C_4O_4)(H_2O)]_2\cdot H_2O$ (**4**), by using flexible dpa (2,2′-dipyridylamine) and squarate ($C_4O_4^{2-}$) ligands as building units, as well as the studies of their thermal stability and magnetic properties.

Results and Discussion

Synthesis and IR Spectroscopy of Compounds 1–4

Compounds **1**–**4** were synthesized by mixing the divalent metal salt MCl_2 (M = Co, Ni, Cu, Zn), 2,2′-dipyridylamine (dpa), $H_2C_4O_4$, and H_2O. All reactions were carried out in 23-mL, acid-digestion bombs at 180 °C for three days. Low pH values were observed in all reactions (final pH = 2.82–3.91). The resulting products are very stable in air at ambient temperature and insoluble in common solvents such as water, alcohol, and acetonitrile. It is also worthy to note that the synthetic reproducibility is high. The appearance of N–H stretching vibrations in the region of 3000–

[a] Department of Chemistry, Soochow University, 111, Taipei, Taiwan
Fax: +886-2-2881-1053
E-mail: ccwang@mail.scu.edu.tw
[b] Instrumentation Center, National Taiwan University, Taipei, Taiwan
[c] Department of Chemistry, National Cheng Kung University, Tainan, Taiwan

3400 cm^{-1} in the IR spectrum is in agreement with that reported for hydrogen bonds between N–H and several H-acceptor groups. The most relevant IR features are those associated with the chelating squarate ligands. The coordinated CO groups are characterized by medium-strength absorptions at around 1664 cm^{-1}. A very strong band centered at around 1480 cm^{-1} is attributed to a combination mode of C–O and C–C stretchings and is in agreement with other $(CO)_n^{2-}$ salts.[27]

Crystal Structures of [M(dpa)(C_4O_4)(H_2O)] Complexes

Compounds **1**–**3** were found to be isostructural; a typical structure of **1** is shown in Figure 1. In **1**–**3**, each metal center is six-coordinate and adopts a slightly distorted octahedral coordination environment, being bonded to two nitrogen atoms from dpa ligands and four oxygen atoms from two squarate ligands and two water molecules. The corresponding M–N, M–O_w and M–O_{sq} bond lengths (see Table 1) are similar to those of relevant squarate-bridged metal complexes.[19–21,28,29] Two metal centers are linked together by two bridging water molecules to form an $[M(dpa)(H_2O)]_2^{4+}$ dimeric fragment (see Figure 1) in the equatorial plane. The squarate ligand adopts a $\mu_{1,2}$-binding mode to connect the neighboring $[M(dpa)(\mu_2\text{-}OH_2)]_2$ fragments at the axial sites, constructing a 1D linear two-legged ladder-like metal–organic framework (MOF) along the *a* axis [see (a) in Figure 2]. The M···M separations via μ_2-O_{water} and $\mu_{1,2}$-$C_4O_4^{2-}$ bridges are 3.459(1) and 7.416(1) Å

Table 1. Selected bond lengths [Å] and angles [°] for compounds **1**–**3**.[a]

	1 [M = Co]	**2** [M = Ni]	**3** [M = Zn]
M(1)–O(1)	2.081(1)	2.073(1)	2.096(1)
M(1)–O(2)	2.119(1)	2.096(1)	2.148(1)
M(1)–O(5)	2.155(2)	2.105(2)	2.133(1)
M(1)–$O(5)_i$	2.213(2)	2.175(2)	2.282(1)
M(1)–N(1)	2.121(2)	2.075(2)	2.117(2)
M(1)–N(3)	2.095(2)	2.056(2)	2.088(1)
C(1)–O(1)	1.256(3)	1.255(2)	1.261(2)
C(2)–$O(2)_{ii}$	1.251(3)	1.248(2)	1.256(2)
C(3)–O(3)	1.252(3)	1.257(2)	1.255(2)
C(4)–O(4)	1.270(2)	1.270(2)	1.270(2)
C(1)–C(2)	1.477(3)	1.475(3)	1.471(2)
C(2)–C(3)	1.474(3)	1.476(3)	1.471(2)
C(3)–C(4)	1.456(3)	1.449(3)	1.454(2)
C(4)–C(1)	1.454(3)	1.461(3)	1.452(2)
O(1)–M(1)–O(2)	176.37(6)	174.43(6)	174.35(5)
O(1)–M(1)–O(5)	91.53(6)	92.46(6)	92.06(5)
O(1)–M(1)–$O(5)_i$	90.11(6)	90.09(6)	89.32(5)
O(1)–M(1)–N(1)	92.50(6)	92.29(6)	93.66(5)
O(1)–M(1)–N(3)	90.55(6)	89.04(6)	90.34(5)
O(2)–M(1)–O(5)	90.54(6)	91.77(6)	90.22(5)
O(2)–M(1)–$O(5)_i$	87.54(6)	87.48(6)	86.27(5)
O(2)–M(1)–N(1)	90.07(6)	90.62(7)	91.03(5)
O(2)–M(1)–N(3)	86.93(6)	86.18(6)	86.47(5)
O(5)–M(1)–$O(5)_i$	75.25(6)	75.22(6)	75.15(5)
O(5)–M(1)–N(1)	100.01(7)	99.14(6)	99.99(5)
O(5)–M(1)–N(3)	170.54(7)	170.09(6)	169.01(5)
O(5)i–M(1)–N(1)	174.65(7)	173.98(6)	174.40(5)
O(5)i–M(1)–N(3)	95.52(7)	94.99(6)	94.17(5)
N(1)–M(1)–N(3)	89.12(7)	90.58(7)	90.55(6)

[a] Symmetry operations used to generate equivalent atoms: (i) $-x, -y, -z$; (ii) $x + 1, y, z$.

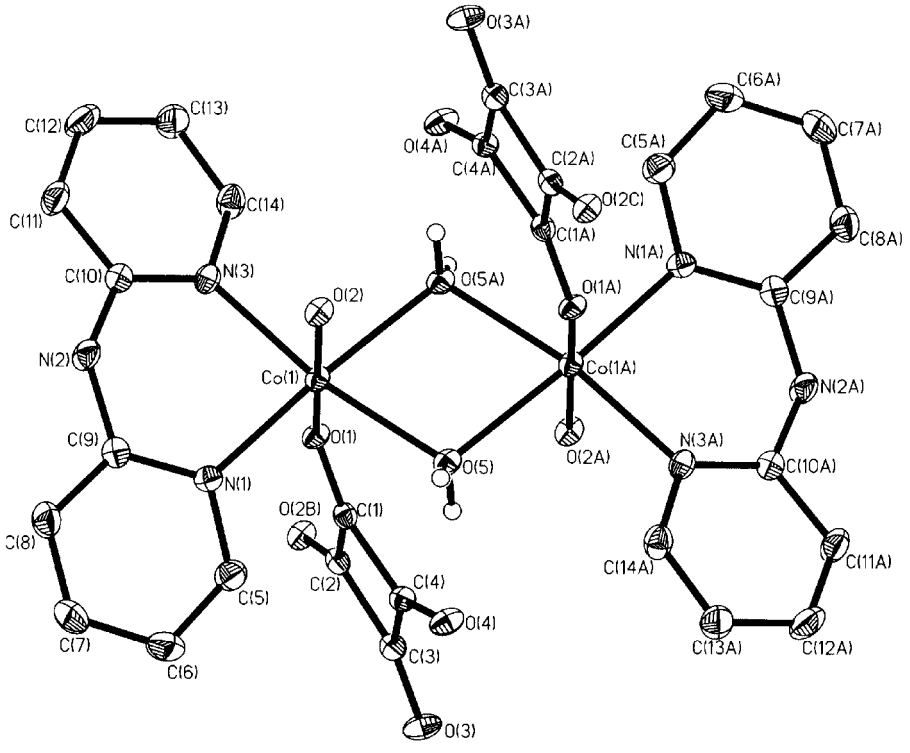

Figure 1. The basic building block of compound **1** showing the atom numbering scheme. Ellipsoids are drawn at the 50% probability level. Symmetry codes: A ($-x, -y, -z$), B ($1 + x, y, z$), C ($-1 - x, -y, -z$).

for **1**, 3.391(1) and 7.377(1) Å for **2**, and 3.501(1) and 7.458(1) Å for **3**. The corresponding C–C and C–O bond lengths (see Table 1) of the squarate ligands show a roughly D_{4h} delocalized mode and fall in the same range as some analogous squarate-bridged complexes.[19–21,29] It should be noted that adjacent ladders are displaced by half a repeating unit along the *a* and *c* axes. This arrangement effectively prevents steric hindrance between the inter-ladder dpa ligands. As a result, compounds **1**–**3** favor the closer-packed building block shown in Figure 2. The centroids of the pyridine rings in the dpa ligands of adjacent ladders are generally parallel and adopt a face-to-face alignment with a separation distance within the range 3.59–3.82 Å, thus indicating a weak π–π stacking interaction[28,30] that may, in part, contribute to the stabilization of the extended framework. Hydrogen-bond formation is a very important aspect in constructing coordination polymers.[31–35] In compounds **1**–**3**, two strong O–H···O hydrogen bonds [O(5)–H(5a)···O(4) and O(5)–H(5b)···O(3)] are found between uncoordinated oxygen atoms of squarate and the coordinated water molecules, with O···O distances in the range of 2.528–2.600 Å, which are similar to those (2.589–2.748 Å) of O_{sq}···O_w-type hydrogen bonds found in other squarate-bridged compounds.[19–22,28b] In addition, the inter-ladder interactions are through one pair of N–H···O [N(2)–H(2a)···O(4)] and C–H···O [C(11)–H(11a)···O(4)] hydrogen bonds from the same dpa molecule linked to the oxygen atom of squarate in the neighboring ladders to form a mixed N–H···O and C–H···O hydrogen bond (dashed line in Figure 2(b)]. A similar hydrogen-bonding interaction has also been found in complexes such as [Fe(ox)(dpa)][28a] and $[M_2(dpa)_2(C_2O_4)(C_4O_4)]$.[28b] Relevant bond lengths and angles of the O–H···O, N–H···O and C–H···O hydrogen bonds for **1**–**3** are summarized in Table 2.

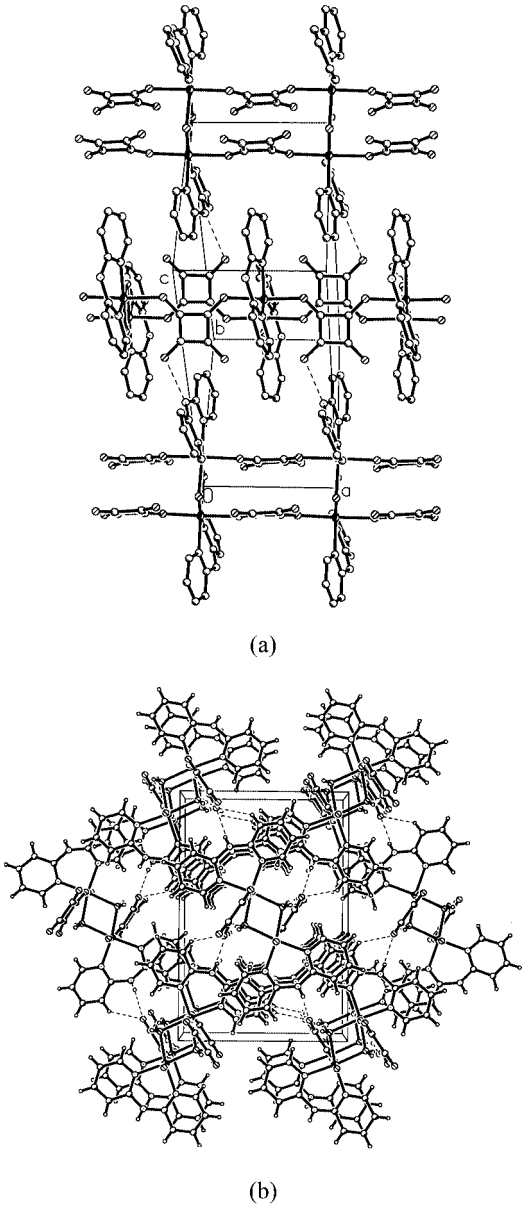

Figure 2. Perspective view of compound **1** along the crystallographic *b* axis (a) and the *a* axis (b).

Crystal Structure of $[Cu(dpa)(C_4O_4)(H_2O)]_2\cdot(H_2O)$ (4)

The asymmetric unit of compound **4** contains two copper ions, two squarates, two dpa ligands, and one solvated, doubly coordinated water molecule. Each of the two independent Cu centers adopts a slightly distorted square-pyramidal coordination environment, but is subject to different environments incorporating squarate and water molecules (Figure 3). In the equatorial plane, Cu(1) is bonded to two nitrogen atoms of dpa and two oxygen atoms of the two squarate ligands, while Cu(2) is bonded to two nitrogen atoms of dpa and two oxygen atoms, one from $C_4O_4^{2-}$ and the other from the water molecule. The axial ligand bonded to Cu(1) is the oxygen atom of a water molecule [O(9)], while that bonded to Cu(2) is an oxygen atom of a squarate [O(6)], forming a distorted square-pyramidal coordination environment. A 1D helical chain is observed in which the copper ions are alternately bridged by equatorial-axial and equatorial-equatorial $\mu_{1,2}$-$C_4O_4^{2-}$ ligands (Figure 4). The Cu···Cu separations across the equatorial-axial and equatorial-equatorial $C_4O_4^{2-}$ bridges are 4.832(4) Å and 5.392(4) Å, respectively. The former is longer than that of 4.328(1) Å in $[Cu(C_4O_4)(C_4H_4N_2)]_n$[36] but shorter than other relevant $\mu_{1,2}$- or $\mu_{1,2,3,4}$-$C_4O_4^{2-}$-bridged Cu complexes.[19a,22,26b,37] As expected, the axial Cu(1)–$O(9)_w$ and Cu(2)–$O(6)_{sq}$ distances of 2.242(2) and 2.174(2) Å are significantly longer than the equatorial Cu(1)–$O(1)_{sq}$ and Cu(1)–$O(5)_{sq}$ bond lengths [2.026(2) and 1.955(2) Å respectively] and the Cu(2)–$O(2)_{sq}$ and Cu(2)–$O(10)_w$ bond lengths [2.013(2) and 1.954(2) Å respectively] due to the Jahn–Teller distortion. The corresponding Cu–O_w, Cu–O_{sq}, and Cu–N bond lengths listed in Table 3 are similar to those found in some other squarate-bridged Cu complexes.[22–26,32,37] Hydrogen bonds also play an important role in the helical chain of compound **4**. These include three O–H···O hydrogen bonds [O(11)–H(11a)···O(8), O(10)–H(10b)···O(11), and O(9)–H(9b)···O(2)] between water molecules and squarate ligands, with O···O distances

Table 2. Hydrogen bonds for compounds **1**–**3**.[a]

	Donor–H [Å]	Donor···Acceptor [Å]	H···Acceptor [Å]	∠Donor–H···Acceptor [°]
	O(5)–H(5a)	O(5)···O(4)	H(5a)···O(4)	∠O(5)–H(5a)···O(4)
1 [Co]	0.795(3)	2.574	1.784	172.6
2 [Ni]	0.812(3)	2.568	1.764	170.5
3 [Zn]	0.874(2)	2.584	1.712	174.8
	O(5)–H(5b)	O(5)···O(3)$_i$	H(5b)···O(3)$_i$	∠O(5)–H(5b)···O(3)$_i$
1 [Co]	0.760(4)	2.528	1.829	170.7
2 [Ni]	0.839(3)	2.574	1.738	174.6
3 [Zn]	0.891(3)	2.587	1.713	166.1
	N(2)–H(2a)	N(2)···O(4)$_{ii}$	H(2a)···O(4)$_{ii}$	∠N(2)–H(2a)···O(4)$_{ii}$
1 [Co]	0.860(2)	2.874	2.074	154.5
2 [Ni]	0.859(2)	2.871	2.080	152.6
3 [Zn]	0.860(2)	2.869	2.076	153.1
	C(11)–H(11a)	C(11)···O(4)$_{ii}$	H(11a)···O(4)$_{ii}$	∠C(11)–H(11a)···O(4)$_{ii}$
1 [Co]	0.929(3)	3.231	2.465	139.9
2 [Ni]	0.930(2)	3.248	2.486	139.3
3 [Zn]	0.931(2)	3.234	2.467	139.8

[a] Symmetry operations used to generate equivalent atoms: (i) –1 + *x*, *y*, *z*; (ii) –0.5 + *x*, 0.5 – *y*, 0.5 + *z*.

in the range 2.588–2.785 Å, similar to those (2.589–2.748 Å) of O_{sq}···O_w-type hydrogen bonds found in other squarate-bridged compounds.[19–22] The inter-chain interactions are through hydrogen bonds between the dpa nitrogen atoms in one chain and uncoordinated squarate oxygen atoms in the adjacent chain, with hydrogen-bonding distances N(2)–H(2a)···O(3)$_{ii}$ of 2.776 Å and N(5)–H(5a)···O(4)$_{iii}$ of 2.961 Å (dashed line in Figure 4). Relevant bond lengths and angles of the O–H···O and N–H···O hydrogen bonds for complex **4** are listed in Table 4.

Magnetic Properties

Compound 2

Plots of the magnetic susceptibility (χ_M and $\chi_M T$) in the temperature range of 5–300 K for **2** are shown in Figure 5. At room temperature, the $\chi_M T$ value is 2.31 emu K mol^{-1}, which, upon cooling, slowly decreases to a value of 2.05 emu K mol^{-1} at 75 K and then drops rapidly from 1.66 emu K mol^{-1} at 30 K to 0.35 emu K mol^{-1} at 5 K. This seems to be characteristic of weakly antiferromagnetic be-

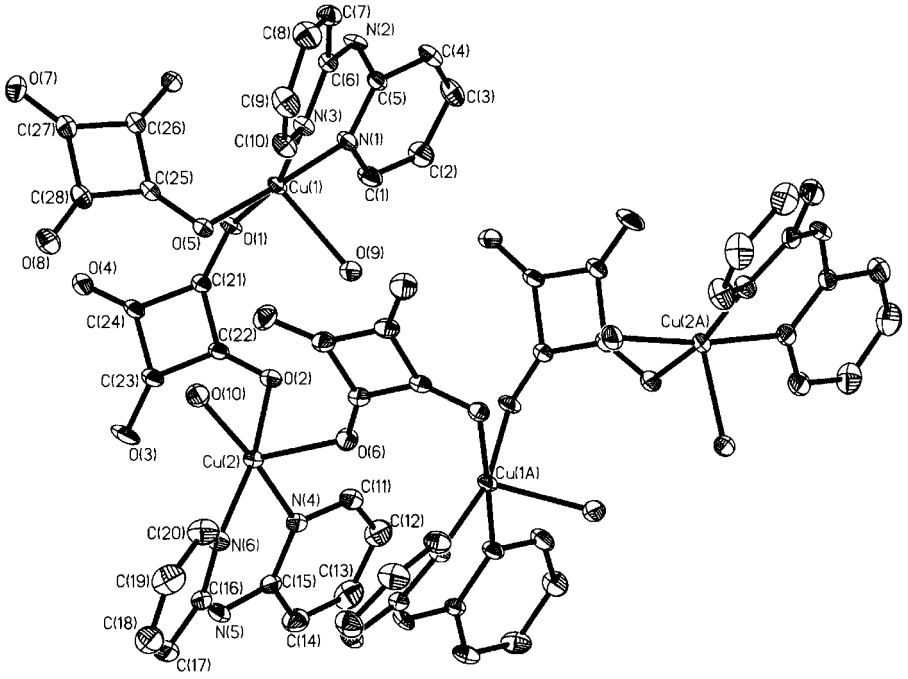

Figure 3. The basic building block of compound **4** showing the atom numbering scheme. Ellipsoids are drawn at the 50% probability level. Symmetry codes: A (–0.5 – *x*, –0.5 + *y*, *z*).

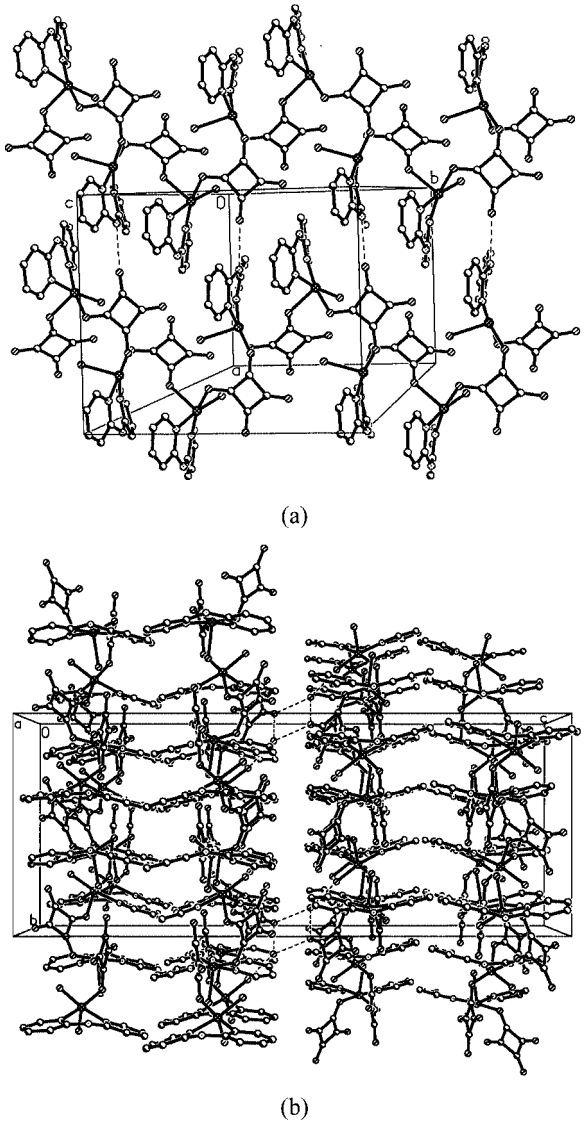

Figure 4. Perspective view of compound **4** along the crystallographic *c* axis (a) and the *a* axis (b).

havior. In order to analyze the magnetic exchange coupling interaction in **2**, the susceptibility data was fitted to a binuclear magnetic model, namely a dimer formed by double μ-OH_2 bridges, $[(dpa)Ni(\mu_2\text{-}OH_2)_2Ni(dpa)]^{4+}$. The corresponding molar susceptibility was calculated from the Hei-

Table 3. Selected bond length [Å] and angles [°] for compound **4**.[a]

Cu(1)–O(1)	2.026(2)	Cu(2)–O(2)	2.013(2)
Cu(1)–O(5)	1.955(2)	Cu(2)–O(6)	2.174(2)
Cu(1)–O(9)	2.242(2)	Cu(2)–O(10)	1.954(2)
Cu(1)–N(1)	1.984(2)	Cu(2)–N(4)	1.985(2)
Cu(1)–N(3)	2.014(2)	Cu(2)–N(6)	1.991(2)
C(21)–O(1)	1.274(3)	C(25)–O(5)	1.270(3)
C(22)–O(2)	1.272(3)	$C(26)–O(6)_i$	1.254(3)
C(23)–O(3)	1.237(3)	C(27)–O(7)	1.237(3)
C(24)–O(4)	1.249(3)	C(28)–O(8)	1.241(3)
C(21)–C(22)	1.444(3)	C(25)–C(26)	1.448(3)
C(22)–C(23)	1.449(3)	C(26)–C(27)	1.476(3)
C(23)–C(24)	1.477(3)	C(27)–C(28)	1.475(4)
C(24)–C(21)	1.464(3)	C(28)–C(25)	1.454(3)
O(5)–Cu(1)–N(1)	175.64(8)	O(10)–Cu(2)–N(4)	169.4(1)
O(5)–Cu(1)–N(3)	91.92(8)	O(10)–Cu(2)–N(6)	92.4(1)
N(1)–Cu(1)–N(3)	90.62(7)	N(4)–Cu(2)–N(6)	89.19(8)
O(5)–Cu(1)–O(1)	85.53(7)	O(10)–Cu(2)–O(2)	85.30(9)
N(1)–Cu(1)–O(1)	91.08(7)	N(4)–Cu(2)–O(2)	91.04(8)
N(3)–Cu(1)–O(1)	164.31(8)	N(6)–Cu(2)–O(2)	168.24(8)
O(5)–Cu(1)–O(9)	93.88(8)	O(10)–Cu(2)–O(6)	95.28(9)
N(1)–Cu(1)–O(9)	89.33(9)	N(4)–Cu(2)–O(6)	94.73(7)
N(3)–Cu(1)–O(9)	96.87(9)	N(6)–Cu(2)–O(6)	100.26(8)
O(1)–Cu(1)–O(9)	98.75(8)	O(2)–Cu(2)–O(6)	91.43(7)

[a] Symmetry operations used to generate equivalent atoms: (i) $-x + 1/2, y - 1/2, z$.

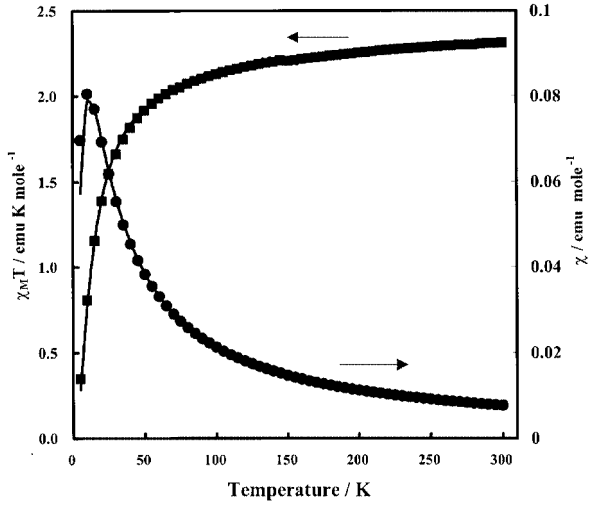

Figure 5. Plots of χ_M (●) and $\chi_M T$ (■) vs. T [K] for **2**. The solid line represents the best theoretical fit.

Table 4. Hydrogen bonds for compound **4**.[a]

Donor–H [Å]		Donor···Acceptor [Å]		H···Acceptor [Å]		∠ Donor–H···Acceptor [°]	
O(11)–H(11a)	0.950(4)	$O(11)\cdots O(8)_i$	2.759	$H(11a)\cdots O(8)_i$	1.939	$\angle O(11)–H(11a)\cdots O(8)_i$	143.1
O(11)–H(11b)	0.774(4)	O(11)···O(8)	2.785	H(11b)···O(8)	2.017	∠O(11)–H(11b)···O(8)	171.1
O(10)–H(10b)	0.895(4)	O(10)···O(11)	2.588	H(10b)···O(11)	1.707	∠O(10)–H(10b)···O(11)	167.3
O(9)–H(9b)	0.815(3)	O(9)···O(2)	2.768	H(9b)···O(2)	2.122	∠O(9)–H(9b)···O(2)	136.1
N(2)–H(2a)	0.860(2)	$N(2)\cdots O(3)_{ii}$	2.776	$H(2a)\cdots O(3)_{ii}$	2.033	$\angle N(2)–H(2a)\cdots O(3)_{ii}$	144.2
N(5)–H(5a)	0.860(2)	$N(5)\cdots O(4)_{iii}$	2.961	$H(5a)\cdots O(4)_{iii}$	2.263	$\angle N(5)–H(5a)\cdots O(4)_{iii}$	138.4

[a] Symmetry operations used to generate equivalent atoms: (i) $1 - x, -y, 1 - z$; (ii) $1 + x, y, z$; (iii) $1.5 - x, 0.5 + y, z$.

senberg model ($H = -2JS_1S_2$, $S_1 = S_2 = 1$) given in Equation (1)[42]

$$\chi'_M = \frac{Ng^2\beta^2}{kT}\frac{2\exp(x)+10\exp(3x)}{1+3\exp(x)+5\exp(6x)} + TIP \quad (1)$$

where N, g, β, and x are the Avogadro number, g factor, Bohr magneton, and J/kT, respectively; TIP is the temperature-independent paramagnetism of the Ni^{2+} ion. The best fitting results for magnetic susceptibility data give $TIP = 4.00\times10^{-4}$ emu mol^{-1}, $g = 2.13$, $J = -3.9$ cm^{-1}, and $R = 2.80\times10^{-5}$ [$R = \Sigma[(\chi_M T)_{obs} - (\chi_M T)_{cal}]^2/\Sigma(\chi_M T)^2_{obs}$]. As shown in Figure 5, the solid lines obtained from the theoretical approach are in good agreement with the experimental results. The negative value of J, according to the crystallographic results, indicates an antiferromagnetic interaction through the water bridges between Ni^{II} ions in the [(dpa)-Ni(μ_2-OH$_2$)$_2$Ni(dpa)] dimer and the spin-orbit coupling contributes trivially to the g factor. The intermolecular exchange interactions through $\mu_{1,2}$-squarate bridges can be ignored since there is only a weak antiferromagnetic interaction through the squarate bridge in [Ni(C$_4$O$_4$)(tren)(H$_2$O)$_2$](ClO$_4$)$_2$ ($J = -0.4$ cm^{-1}).[19]

Compound 4

The temperature dependence of the magnetic susceptibilities of **4** in the form of χ_M and $\chi_M T$ vs. T plots is shown in Figure 6. At room temperature, the $\chi_M T$ value is 0.89 emu K mol^{-1}, which is equal to the spin-only $\chi_M T$ value of 0.89 when $g = 2.18$, expected for a doubly uncoupled $S = 1/2$ system. As the temperature decreases, the $\chi_M T$ value remains nearly unchanged and finally reaches a value of 0.88 emu K mol^{-1} at 5 K. This magnetic behavior indicates the existence of a very weak antiferromagnetic interaction between the Cu^{II} ions. Based on the framework of compound **4**, two possible origins of the magnetic properties are tentatively proposed, namely the magnetism induced from either the equatorial-axial squarate bridge with a separation distance of 4.832(4) Å or the equatorial-equatorial squarate bridge separated by 5.392(4) Å. In either case, the magnetic interaction is mainly dominated by the equatorial-axial squarate bridge. As a result, the magnetic susceptibility data can be fitted with the binuclear magnetic model to give $TIP = 0.0$ emu mol^{-1}, $g = 2.18$, $J = -0.08$ cm^{-1} and $R = 9.24\times10^{-6}$. The solid lines obtained from the theoretical model in Figure 6 demonstrate a good agreement between the theoretical and experimental results. For complex **4**, the magnetic interaction via the squarate bridge is rather small and it can thus be treated as a paramagnetic ion because of the weak overlap between the magnetic orbital through the $\mu_{1,2}$-bis-monodentate squarate bridging ligands.[24] However, the magnetic susceptibility data can be fitted to a Curie–Weiss law with $\theta = +0.224$ K, and $C = 0.444$ emu K mol^{-1}. The Curie constant agrees well with the value of $g = 2.18$ for a copper(II) one-spin electron configuration, which corresponds to a value of $\chi_M T$ per copper ion of 0.89 emu K mol^{-1}. The small, positive Weiss constant does not really reflect a weak ferromagnetic interaction but rather implies that there is a lack of strong metal–metal interactions within the frameworks.

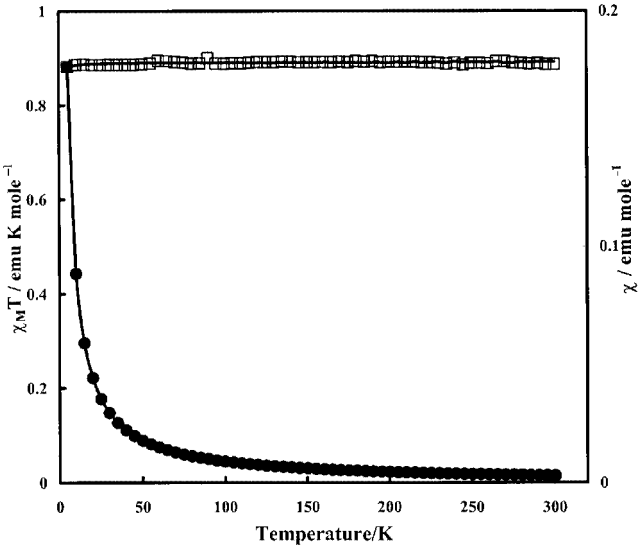

Figure 6. Plots of χ_M (●) and $\chi_M T$ (□) vs. T [K] for **4**. The solid line represents the best theoretical fit.

Compound 1

The magnetic behavior of **1** is illustrated in Figure 7 as a plot of $\chi_M T$ as a function of temperature in the range 5–300 K. At room temperature, the $\chi_M T$ value is 3.94 emu K mol^{-1}, which is close to the value (3.76 cm^3 K mol^{-1}) of a doubly uncoupled $S = 3/2$ spin system. The value of $\chi_M T$ slowly increases as the temperature decreases, and reaches a maximum (4.18 emu K mol^{-1}) near 125 K. It then decreases continuously and finally reaches a value of 1.52 emu K mol^{-1} at 5 K. For a weak-field configuration ($A = 1.5$) the value of $\chi_M T$ (3.94 emu K mol^{-1}) is unexpectedly large. Note that a similar phenomenon has been reported in the case of $CoBr_2$.[39] From the geometry point

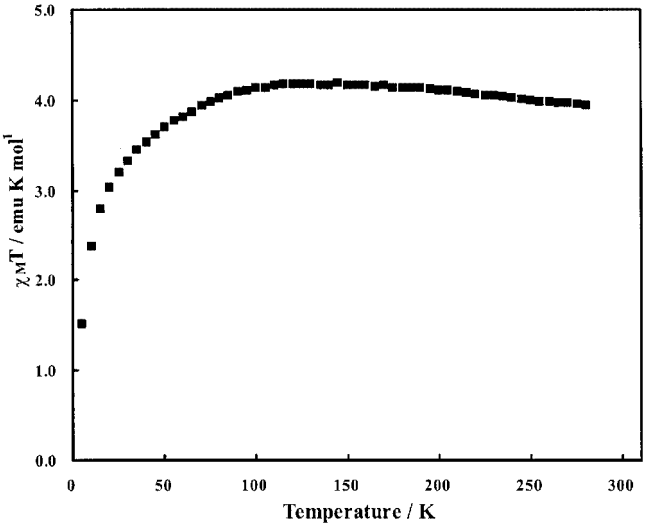

Figure 7. Plots of $\chi_M T$ (■) vs. T [K] for **1**.

of view, the magnetic behavior may originate from the antiferromagnetic dimers $[(dpa)Co(\mu_2\text{-}OH_2)_2Co(dpa)]^{4+}$, bridged by H_2O ligands [Co···Co separation of 3.459(1) Å] similar to that of complex **2**. However, the susceptibility data could not be analyzed by using an expression for the magnetic susceptibility of a dinuclear cobalt(II) system because the dinuclear system does not take into account the effects of the zero-field splitting and/or spin-orbital coupling, which may be significant for cobalt(II) ions.[38,40]

Thermogravimetric Analysis

To assess the thermal stability of compounds **1**–**4** and their structural variation as a function of the temperature, thermogravimetric analysis (TGA) was performed on single-phase polycrystalline samples for each compound. The former three compounds (**1**–**3**) all undergo a continuous, single-step weight-loss process (losing coordinated water, followed by detachment of dpa and squarate groups) and are thermally stable up to at least 175 °C. The on-set temperatures for the weight losses are approximately 175 °C, 258 °C, and 180 °C for **1**–**3**, respectively. The decomposition processes were completed at approximately 454 °C for **1**, 361 °C for **2**, and 436 °C for **3**. These samples are then decomposed completely. The final products of the pyrolysis were identified as Co_3O_4, NiO, and ZnO, with remaining percentages of 20.25, 22.25, and 22.92%. The high thermal stability of these compounds can be mainly attributed to the intra- and intermolecular hydrogen bonds in combination with the π-π stacking interaction.

For compound **4**, the dehydration takes place in a temperature range 50–100 °C with a weight lost of 6.6%, corresponding to the calculated value (7.2%) for loss of one solvated and two coordinated water molecules. The loss of squarate groups occurs in the range 210–260 °C, with the weight loss of 30.0% corresponding to the calculated value of 30.5%. Above 290 °C the dpa ligand is degraded. The final pyrolysis product is CuO, with a remaining percentage of 20.98%.

Conclusions

In conclusion, under hydrothermal conditions, we have successfully synthesized two metal coordination polymer frameworks $[M(dpa)(C_4O_4)(H_2O)]$ [M = Co (**1**), Ni (**2**), Zn (**3**)] and $[Cu(dpa)(C_4O_4)(H_2O)]_2{\cdot}H_2O$ (**4**), the structures of which have been well characterized by X-ray diffraction. The squarate ligands afford a $\mu_{1,2}$-bridging coordination mode as well as hydrogen-bonding capability to build a 1D two-legged ladder-like MOF for compounds **1**–**3** and a 1D helical chain for compound **4**. The magnetic studies indicate a weak antiferromagnetic interaction via H_2O bridges for **1** and **2** and paramagnetism for **4**.

Experimental Section

Materials and Physical Techniques: All chemicals were of reagent grade and were used as received. The IR spectra were recorded on a Nicolet Fourier Transform IR, MAGNA-IR 500 spectrometer in the range of 500–4000 cm^{-1} using the KBr disc technique. The magnetic susceptibilities were measured on polycrystalline samples of compound **1** (Co), **2** (Ni), and **4** (Cu) at a field of 10000 G over a temperature range from 5 to 300 K with a SQUID magnetometer. Diamagnetic corrections were made with Pascal's constants for all constituent atoms, and the magnetic moments were calculated by the equation $\mu_{eff} = 2.828(\chi_M T)^{1/2}$. Thermogravimetric analyses (TGA) of the title compounds were performed on a computer-controlled Perkin–Elmer 7 Series/UNIX TGA7 analyzer. Single-phase powder samples of **1** (4.014 mg), **2** (5.079 mg), **3** (1.532 mg), and **4** (4.406 mg) were loaded into alumina pans and heated with a ramp rate of 5 °C min^{-1} from room temperature to 900 °C under nitrogen.

Synthesis of $[Co(dpa)(C_4O_4)(H_2O)]$ (1): Reaction of anhydrous $CoCl_2$ (0.0131 g, 0.1 mmol), $H_2C_4O_4$ (0.0114 g, 0.1 mmol), dpa (0.0348 g, 0.2 mmol), and deionized water (6 mL) in a molar ratio of 1:1:2:3333 at 180 °C for three days produced red, column-like crystals of **1** in a yield of 0.0198 g (54.9%) based on Co^{II}. The final pH value was 3.28. IR (KBr): $\tilde{\nu}$ = 3319 (w), 3204 (w), 3141 (w), 3041 (w), 1651 (m), 1582 (m), 1540 (s), 1480 (vs), 1425 (s), 1379 (m), 1235 (m), 1160 (m), 1011 (m), 847 (w), 763 (m), 646 (w) cm^{-1}. $C_{14}H_{11}CoN_3O_5$ (360.19): calcd. C 46.69, H 3.08, N 11.67; found C 46.78, H 3.01, N 11.64.

Synthesis of $[Ni(dpa)(C_4O_4)(H_2O)]$ (2): Reaction of $NiCl_2{\cdot}6H_2O$ (0.0241 g, 0.1 mmol), $H_2C_4O_4$ (0.0115 g, 0.1 mmol), dpa (0.0352 g, 0.2 mmol), and deionized water (6 mL) in a molar ratio of 1:1:2:3333 at 180 °C for three days produced light-blue, column-like crystals of **2** in a yield of 0.0194 g (53.9%) based on Ni^{II}. The final pH value was 2.82. IR (KBr): $\tilde{\nu}$ = 3319 (w), 3206 (w), 3143 (w), 3043 (w), 1652 (s), 1601 (s), 1580 (s), 1541 (vs), 1486 (vs, broad), 1434 (vs), 1381 (s), 1276 (m), 1236 (m), 1166 (m), 1160 (s), 1081 (m), 1047 (m), 1015 (m), 900 (m), 851 (m), 789 (m), 763 (m), 648 (w) cm^{-1}. $C_{14}H_{11}N_3NiO_5$ (359.97): calcd. C 46.72, H 3.08, N 11.67; found C 46.87, H 2.92, N 11.76.

Synthesis of $[Zn(dpa)(C_4O_4)(H_2O)]$ (3): Reaction of anhydrous $ZnCl_2$ (0.0136 g, 0.1 mmol), $H_2C_4O_4$ (0.0114 g, 0.1 mmol), dpa (0.0340 g, 0.2 mmol), and deionized water (6 mL) in a molar ratio of 1:1:2:3333 at 180 °C for three days produced light-brown, needle-like crystals of **3** in a yield of 0.0256 g (69.8%) based on Zn^{II}. The final pH value was 3.74. IR (KBr): $\tilde{\nu}$ = 3307 (w), 3210 (w), 3148 (w), 3037 (w), 1644 (m), 1586 (m), 1532 (s), 1483 (vs), 1379 (m), 1272 (w), 1236 (m), 1160 (m), 1013 (m), 765 (m), 648 (w) cm^{-1}. $C_{14}H_{11}N_3O_5Zn$ (366.63): calcd. C 45.86, H 2.02, N 11.46; found C 45.31, H 2.12, N 11.35.

Synthesis of $[Cu(dpa)(C_4O_4)(H_2O)]_2{\cdot}(H_2O)$ (4): Reaction of $CuCl_2{\cdot}6H_2O$ (0.0170 g, 0.1 mmol), $H_2C_4O_4$ (0.0114 g, 0.1 mmol), dpa (0.0170 g, 0.2 mmol), and deionized water (6 mL) in a molar ratio of 1:1:1:3333 at 180 °C for three days produced black, column-like crystals of **4** in a yield of 0.074 g (98.9%) based on Cu^{II}. The final pH value was 2.94. IR (KBr): $\tilde{\nu}$ = 3304 (w), 3204 (w), 3141 (w), 3106 (w), 3041 (w), 1652 (m), 1589 (m), 1520 (vs), 1483 (vs), 1463 (vs), 1434 (m), 1332 (m), 1241 (m), 1157 (m), 1082 (m), 1025 (m), 766 (m), 650 (m) cm^{-1}. $C_{28}H_{24}Cu_2N_6O_{11}$ (747.61): calcd. C 44.98, H 3.08, N 11.67; found C 44.58, H 2.89, N 11.15.

X-ray Crystallographic Study: Single-crystal structure analyses for compounds **1**–**4** were performed on a Siemens SMART diffractometer with a CCD detector with Mo-K_α radiation (λ = 0.71073 Å) at room temperature. A preliminary orientation matrix and unit-cell parameters were determined from three runs of 15 frames each, with each frame corresponding to a 0.3° scan in 10 s, following by spot integration and least-squares refinement. For each structure, data were measured using ω scans of 0.3° per frame

Table 5. Crystal data for Compounds **1**–**4**.

	1	**2**	**3**	**4**
Empirical formula	$C_{14}H_{11}CoN_3O_5$	$C_{14}H_{11}N_3NiO_5$	$C_{14}H_{11}N_3O_5Zn$	$C_{28}H_{24}Cu_2N_3O_5$
Molecular mass	360.19	359.97	366.63	747.61
Crystal system	monoclinic	monoclinic	monoclinic	orthorhombic
Space group	$P2_1/n$	$P2_1/n$	$P2_1/n$	$Pbca$
a [Å]	7.4158(2)	7.3768(2)	7.4583(2)	11.7740(3)
b [Å]	11.1131(4)	11.0999(3)	11.1632(3)	13.8920(4)
c [Å]	16.3588(5)	16.1870(5)	16.2761(4)	35.1467(9)
β [°]	91.464(1)	91.337(1)	91.494(1)	
V [Å^3]	1347.73(7)	1325.06(6)	1354.66(6)	5748.7(3)
Z	4	4	4	8
$D_{calcd.}$ [g cm^{-3}]	1.775	1.804	1.798	1.728
T [K]	295(2)	295(2)	295(2)	295(2)
μ [mm^{-1}]	1.306	1.497	1.845	1.555
Refl. collected	11321	11512	13735	46336
Refl. unique/R_{int}	3102/0.0321	3048/0.0348	3120/0.0248	6606/0.0367
Refl. with [$I > 2\sigma(I)$]	2291	2269	2499	4894
N_v	216	216	216	448
R_F[a] R_w[b] (all data)	0.0516, 0.0772	0.0503, 0.0654	0.0339, 0.0615	0.0304, 0.0793
R_F[a] R_w[b] [$I > 2\sigma(I)$]	0.0308, 0.0726	0.0295, 0.0612	0.0235, 0.0592	0.0510, 0.0906
Goodness-of-fit	1.011	1.004	1.029	1.076
$\Delta\rho_{max./min.}$ [e Å^{-3}]	+0.377/–0.355	+0.344/–0.414	+0.335/–0.289	+0.332/–0.370

[a] $R_F = \Sigma||F_o| - |F_c||/\Sigma|F_o|$. [b] $R_w(|F|^2) = [\Sigma w(|F_o|^2 - |F_c^2|)^2/\Sigma w|F_o|^2]^{1/2}$.

for 20 s until a complete hemisphere had been collected. Cell parameters were retrieved with SMART[41] software and refined with SAINT[42] on all observed reflections. Data reduction was performed with SAINT and corrected for Lorentz and polarization effects. Absorption corrections were applied with the program SADABS.[43] Direct phase-determination and subsequent difference-Fourier map synthesis yielded the positions of non-hydrogen atoms, which were subjected to anisotropic refinements. For **1**–**4**, all hydrogen atoms were generated geometrically (C–H: 0.95) with the exception of the hydrogen atoms of the coordinated water molecules, which were located in the difference Fourier map with the corresponding positions and isotropic displacement parameters being refined. A final full-matrix, least-squares refinement method on F^2 was applied for all observed reflections [$I > 2\sigma(I)$]. All calculations were performed with the SHELXTL-PC V 5.03 software package.[44] Crystal data and details of the data collection and structure refinements for **1**–**4** are summarized in Table 5.

CCDC-205773 (for **1**), -205772 (for **2**), -172057 (for **3**) and -205774 (for **4**) contain the supplementary crystallographic data for this paper. These data can be obtained free of charge from The Cambridge Crystallographic Data Center via www.ccdc.cam.ac.uk/data_request/cif.

Acknowledgments

The authors are grateful for financial support from the National Science Council of the Republic of China (R.O.C).

[1] M. J. Zaworotko, *Chem. Commun.* **2001**, 1–9 and references cited therein.
[2] S. R. Batten, R. Robson, *Angew. Chem. Int. Ed.* **1998**, *37*, 1460–1494.
[3] O. M. Yaghi, H. Li, C. Davis, D. Richardson, T. L. Groy, *Acc. Chem. Res.* **1998**, *31*, 474–484.
[4] P. J. Hagrman, D. Hagrman, J. Zubieta, *Angew. Chem. Int. Ed.* **1999**, *38*, 2638–2684.
[5] O. R. Evans, R.-G. Xiong, Z. Wang, G. K. Wong, W. Lin, *Angew. Chem. Int. Ed.* **1999**, *38*, 536–538.
[6] W. Lin, O. R. Evans, R.-G. Xiong, Z. Wang, *J. Am. Chem. Soc.* **1998**, *120*, 13 272–13 273.
[7] W. Lin, Z. Wang, L. Ma, *J. Am. Chem. Soc.* **1999**, *121*, 11 249–11 250.
[8] Y. K. Shan, R. H. Huang, S. D. Huang, *Angew. Chem. Int. Ed.* **1999**, *38*, 1751–1755.
[9] J. Y. Lu, M. A. Lawandy, J. Li, T. Yuen, C. L. Lin, *Inorg. Chem.* **1999**, *38*, 2695–2704.
[10] A. Ranganathan, V. R. Pedireddi, C. N. R. Rao, *J. Am. Chem. Soc.* **1999**, *121*, 1752–1753.
[11] G. M. Frankenbach, M. A. Beno, A. M. Kini, J. M. Williams, U. Welp, J. E. Thompson, M.-H. Wangbo, *Inorg. Chim. Acta* **1992**, *192*, 195.
[12] A. Weiss, E. Riegler, I. Alt, H. Bohme, C. Robl, *Z. Naturforsch., Teil B* **1986**, *41*, 18.
[13] A. Weiss, E. Riegler, C. Robl, *Z. Naturforsch., Teil B* **1986**, *41*, 1333.
[14] C. Robl, A. Weiss, *Z. Naturforsch., Teil B* **1986**, *41*, 1341.
[15] B. C. Gerstein, M. Habenschuss, *J. Appl. Phys.* **1972**, *43*, 5155.
[16] S. O. H. Gutschke, M. Molinier, A. K. Powell, P. T. Wood, *Angew. Chem. Int. Ed. Engl.* **1997**, *36*, 991–992.
[17] K. J. Lin, K. H. Lii, *Angew. Chem. Int. Ed. Engl.* **1997**, *36*, 2076–2077.
[18] J. Spandl, I. Brüdgam, H. Hartl, *Angew. Chem. Int. Ed.* **2001**, *40*, 4018–4020.
[19] I. Castro, M. L. Calatayud, J. Sletten, F. Lloret, M. Julve, *J. Chem. Soc., Dalton Trans.* **1997**, 811–817.
[20] a) R. Soules, F. Dahan, J.-P. Laurent, P. Castan, *J. Chem. Soc., Dalton Trans.* **1988**, 587–590; b) M. Dan, C. N. R. Rao, *Solid State Sci.* **2003**, *5*, 615–620.
[21] J. A. C. van Ooijen, J. Reedijk, A. L. Spek, *Inorg. Chem.* **1979**, *18*, 1184–1189.
[22] C. E. Xanthopoulos, M. P. Sigalas, G. A. Katsoulos, C. A. Tsipis, C. C. Hadjikostas, A. Terzis, M. Mentzafos, *Inorg. Chem.* **1993**, *32*, 3743–3747.
[23] I. Castro, J. Faus, M. Julve, Y. Journaux, J. Sletten, *J. Chem. Soc., Dalton Trans.* **1991**, 2533–2538.
[24] X. Solans, M. Aguiló, A. Gieizes, J. Faus, M. Julve, *Inorg. Chem.* **1990**, *29*, 775–784.
[25] I. Castro, J. Faus, M. Julve, *Inorg. Chim. Acta* **1990**, *170*, 251–257.

[26] a) P. S. Mukherjee, S. Konar, E. Zangrando, C. Diaz, J. Ribas, N. R. Chaudhuri, *J. Chem. Soc., Dalton Trans.* **2002**, 3471–3476; b) Y. Akhriff, J. Server-Carrió, A. Sancho, J. García-Lozano, E. Escrivá, L. Soto, *Inorg. Chem.* **2001**, *40*, 6832–6840.
[27] M. Ito, R. Weiss, *J. Am. Chem. Soc.* **1963**, *85*, 2580–2584.
[28] a) J. Y. Lu, A. M. Babb, *Inorg. Chim. Acta* **2001**, *318*, 186–190; b) J. Y. Lu, T. J. Schroeder, A. M. Babb, M. Olmstead, *Polyhedron* **2001**, *20*, 2445–2449.
[29] a) C. R. Lee, C. C. Wang, Y. Wang, *Acta Crystallogr, Sect. B* **1996**, *52*, 966–975; b) T. K. Maji, G. Mostafa, S. Sain, J. S. Prasad, N. R. Chaudhuri, *Cryst. Eng. Commun.* **2001**, 37.
[30] C. Janiak, *J. Chem. Soc., Dalton Trans.* **2000**, 3885–3896.
[31] S. B. Ferguson, E. M. Sanford, E. M. Seward, F. Diederich, *J. Am. Chem. Soc.* **1991**, *113*, 5410–5419.
[32] R. H. Groeneman, L. R. MacGillivray, J. L. Atwood, *Inorg. Chem.* **1999**, *38*, 208–209.
[33] J. Y. Lu, T. Paliwala, S. C. Lim, C. Yu, T. Niu, A. J. Jacobson, *Inorg. Chem.* **1997**, *36*, 923–929.
[34] A. J. Blake, S. J. Hill, P. Hubberstey, W. Li, *J. Chem. Soc., Dalton Trans.* **1997**, 913–914.
[35] O. M. Yaghi, H. Li, T. L. Groy, *J. Am. Chem. Soc.* **1996**, *118*, 9096–9101.
[36] C. Näther, I. Jeβ, *Acta Crystallogr., Sect. C* **2001**, *57*, 260–261.
[37] I. Castro, M. L. Calatayud, J. Sletten, F. Lloret, M. Julve, *Inorg. Chim. Acta* **1999**, *287*, 173–180.
[38] a) M. E. Fisher, *Am. J. Phys.* **1964**, *32*, 343; b) O. Kahn, *Molecular Magnetism*, VCH Publishers, New York, **1993**, p. 258.
[39] W. J. de Haas, B. H. Schultz, *Physica* **1939**, *6*, 481.
[40] F. E. Mabbs, D. J. Machin, *Magnetism and Transition Metal Complexes*, Chapman and Hall, London, **1973**.
[41] *SMART V 4.043 Software for CCD Detector System*; Siemens Analytical Instruments Division: Madison, WI, **1995**.
[42] *SAINT V 4.035 Software for CCD Detector System*; Siemens Analytical Instruments Division: Madison, WI, **1995**.
[43] G. M. Sheldrick, *Program for the Refinement of Crystal Structures*; University of Göttingen: Göttingen, Germany, **1993**.
[44] SHELXTL 5.03 (PC-Version), Program Library for Structure Solution and Molecular Graphics; Siemens Analytical Instruments Division: Madison, WI, **1995**.

Received: August 16, 2004

